

RESEARCH ARTICLE

Fabrication and Characterization of 3D Bioprinted Triple-layered Human Alveolar Lung Models

Wei Long Ng^{1,2†}, Teck Choon Ayi^{3†}, Yi-Chun Liu³, Swee Leong Sing¹, Wai Yee Yeong^{1,2*}, Boon-Huan Tan^{3,4}

¹Singapore Centre for 3D Printing, School of Mechanical and Aerospace Engineering, Nanyang Technological University, 50 Nanyang Avenue, 639798, Singapore

²HP-NTU Digital Manufacturing Corporate Lab, 65 Nanyang Avenue, 637460, Singapore

³Defence Medical and Environmental Research Institute, DSO National Laboratories, 27 Medical Drive, 117510, Singapore

⁴Lee Kong Chian School of Medicine, Novena Campus, Nanyang Technological University, 11 Mandalay Road, 308232, Singapore

[†]These authors contributed equally to this work.

Abstract: The global prevalence of respiratory diseases caused by infectious pathogens has resulted in an increased demand for realistic *in-vitro* alveolar lung models to serve as suitable disease models. This demand has resulted in the fabrication of numerous two-dimensional (2D) and three-dimensional (3D) *in-vitro* alveolar lung models. The ability to fabricate these 3D *in-vitro* alveolar lung models in an automated manner with high repeatability and reliability is important for potential scalable production. In this study, we reported the fabrication of human triple-layered alveolar lung models comprising of human lung epithelial cells, human endothelial cells, and human lung fibroblasts using the drop-on-demand (DOD) 3D bioprinting technique. The polyvinylpyrrolidone-based bio-inks and the use of a 300 µm nozzle diameter improved the repeatability of the bioprinting process by achieving consistent cell output over time using different human alveolar lung cells. The 3D bioprinted human triple-layered alveolar lung models were able to maintain cell viability with relative similar proliferation profile over time as compared to non-printed cells. This DOD 3D bioprinting platform offers an attractive tool for highly repeatable and scalable fabrication of 3D *in-vitro* human alveolar lung models.

Keywords: 3D bioprinting; 3D printing; Biofabrication; Lung bioprinting; *In-vitro* human tissue models; Drop-on-demand

*Correspondence to: Wai Yee Yeong, Singapore Centre for 3D Printing, School of Mechanical and Aerospace Engineering, Nanyang Technological University, 50 Nanyang Avenue, Singapore 639798; wyyeong@ntu.edu.sg

Received: December 22, 2020; **Accepted:** January 28, 2021; **Published Online:** April 9, 2021

Citation: Ng WL, Ayi TC, Liu YC, *et al.*, 2021, Fabrication and Characterization of 3D Bioprinted Triple-layered Human Alveolar Lung Models. *Int J Bioprint*, 7(2):332. <http://doi.org/10.18063/ijb.v7i2.332>

1. Introduction

With the increase in respiratory diseases over the last two decades^[1-4], it is critical to elucidate how these pathogens interact and penetrate through the pulmonary epithelial tissue barrier and evaluate the potential severity of these respiratory diseases. As such, numerous *in-vitro* alveolar lung models ranging from simple, mono-cultured two-dimensional (2D) models^[5] to more sophisticated three-dimensional (3D) constructs^[6] have been developed to closely emulate the human pulmonary epithelial tissue barrier. The 3D tissue constructs are considered more

advanced Biosystems by facilitating critical cell-cell and cell-matrix interactions found within the native tissue and its microenvironment^[7]. The main drawback of these 3D tissue constructs is that the conventional manual production of *in-vitro* tissue models is often laborious and unrepeatable.

3D bioprinting has emerged as one of the leading manufacturing platforms for automated fabrication of highly complex 3D tissues and/or organs in a scalable manner^[8-11]. The envisioned long-term goal of 3D bioprinting is to fabricate highly-functional 3D tissue-engineered constructs in a layer-by-layer fabrication approach^[12,13]. This would promote important cell-extracellular matrix (ECM) and cell-

cell interactions and emulate the sophisticated structures of ECM within the 3D tissue-engineered constructs^[14-16]. Despite being in the early stages of infancy, 3D bioprinting presents tremendous potential for automated fabrication of highly-complex 3D tissue constructs in a scalable and repeatable manner^[17,18]. To date, 3D bioprinting systems have been used to fabricate several 3D tissue constructs such as bone^[19-21], cardiac^[22-24], cartilage^[25-27], liver^[28-30], lung^[31,32] and skin^[33-38]. The 3D bioprinting systems can be categorized into three distinct processes; namely extrusion-based^[39-43], jetting-based^[44-47], and vat polymerization^[48-51], and the choice of a suitable bioprinting process is dependent on the desired application. The use of jetting-based bioprinting process is attractive for drop-on-demand (DOD) patterning of different types of living cells and biomaterials on the same planar surface to achieve thin cellular layers in a contactless and high-throughput manner.

A recent study reported the fabrication of two-cell layered blood-air barrier system consisting of an upper alveolar epithelial layer, a middle layer of Matrigel basement membrane, and a lower endothelial cell layer using jetting-based bioprinting^[31]. The bioprinted blood-air barrier models (~20 µm thickness) were cultured over a period of 3 days and exhibited ordered and homogeneous layer-by-layer organization. However, the study lacked information on the long-term survivability of the 3D blood-air barrier models beyond 3 days post-bioprinting. Several publications have reported the importance of lung fibroblasts for promoting alveolar epithelial proliferation through secretion of hepatocyte growth factors^[52-54]. We hypothesize that co-culture with fibroblasts may aid the survivability of a bioprinted model by promoting cell proliferation to replace injured or dead cells. The fabrication of 3D alveolar lung tissue models requires high survivability rates over a long-term period of at least 14 days, which is critical for potential experimentation with viral infection and translocation studies. The different pathogens that have been studied in lung tissue models include *Pseudomonas aeruginosa* (up to 6 h)^[55], *Yersinia pseudotuberculosis* (up to 4 days)^[56], *Staphylococcus aureus*, and *Burkholderia (Pseudomonas) cepacia* (up to 12 days)^[57]. Furthermore, while the effect of respiratory viral infection becomes measurable 2 – 5 days post-infection, the observation of trans-epithelial electrical resistance and lactate dehydrogenase release may take up to 11 days for some viruses, as the tissue slowly recovers^[58]. The long-term survivability of the *in-vitro* 3D blood-air barrier models is necessary for pathogen proliferation and host responses, for example, induced gene expression, secretion of cytokines, or cell death. Furthermore, the overall thickness of the native pulmonary blood-air barrier is only ~1.6 µm^[59] and the current drawbacks of most existing 3D alveolar lung tissue constructs are the inclusion of a relatively thick and porous membrane (i.e., polyester membrane ~ 10 µm thickness) found between the lung epithelial cells and endothelial cell layers^[60-64]. A study has

shown that the presence of this porous synthetic membrane impeded nanoparticle translocation^[64]. Hence, it is possible that virus translocation across these blood-air barrier models may also be impeded by the same synthetic membrane due to non-specific adsorption.

In this study, we demonstrated the ability to fabricate *in-vitro* 3D bioprinted human alveolar lung models in a highly automated and repeatable manner using DOD bioprinting approach. The main contribution of this study is to demonstrate consistent and uniform cell printing for multiple cell printing over a relatively long period. The 3D bioprinted human alveolar lung models consisting of collagen matrix, alveolar lung epithelial, endothelial, and fibroblast cells are successfully fabricated and characterized in this study. The cell suspensions were first modified with 2.5% w/v polyvinylpyrrolidone (PVP)-based bio-inks and printed using a suitable nozzle diameter of 300 µm to prevent clogging issues and ensure a relatively consistent cell output over a period of 30 min. The printed cells maintained high cell viability and exhibited similar proliferation profile over time as compared to non-printed cells and the 3D bioprinted triple-layered human alveolar lung models can be cultured over a period of 14 days with high survivability rates.

2. Materials and methods

2.1. Cell culture

Three different types of human lung cell lines were purchased from ATCC®: A549 human lung epithelial cells (ATCC® CCL-185), EA.hy926 human endothelial cells (ATCC® CRL-2922), and MRC5 human lung fibroblasts (ATCC® CCL-171). These cell lines have been used by others for building *in-vitro* models of the lung alveolar^[31,61,65-67]. The A549 cells were cultured in RPMI-1640 culture medium (Gibco™ Thermo Fisher Scientific) supplemented with 10% fetal bovine serum (FBS, ATCC 302020) and 100 U/ml of penicillin-streptomycin (pen-strep, ATCC 30-2300) solution^[31]. The EA.hy926 and MRC-5 cells were cultured in DMEM/F12 culture medium supplemented with 10% FBS and 100 U/ml of pen-strep solution^[68,69]. The A549 culture medium used in this study were based on a previous work^[31] and it was known that DMEM/F12 can support the growth of either EaHy926 or MRC5^[68,69]. The culture medium was changed once every 3 days and the cells were routinely passaged in tissue culture flasks (passages 3 – 5), with the adherent cells harvested using 0.25% trypsin/ethylene diamine tetra-acetic acid (EDTA) (ATCC 302101) at 90% confluency.

(1) Co-culture medium for different types of human alveolar cells

This is the first study that incorporates these three different kinds of alveolar lung cells together. After some optimization, a 1:1 v/v combination of RPMI 1640 and

DMEM/F12 was found to support the co-culture of A549, EA.hy926 and MRC5. Hence, the cell proliferation profile in the proposed co-culture medium was evaluated against their respective recommended medium (benchmark). Before the bioprinting process, the three different types of human pulmonary cell lines were cultured individually in the co-culture medium (1:1 v/v of RPMI-1640 to DMEM/F12 culture medium – Gibco™ Thermo Fisher Scientific) and their respective culture medium (control medium), to assess the suitability of the co-culture medium to support the growth of the different cell types. The PrestoBlue® assay (Invitrogen™ A13262, Thermo Fisher Scientific) was used to measure cell proliferation based on the normalized relative fluorescence units over a period of 7 days; with the cell morphologies and proliferation rates serving as indicators for determining the suitability of the co-culture medium.

2.2. Fabrication of 3D bioprinted triple-layered human alveolar lung models

(1) DOD bioprinting of cell droplets

A common problem for jetting-based bioprinting process is cell sedimentation where the gravitational forces acting on the floating cells can lead to poor cell homogeneity within the printing cartridge over time. As such, different cell suspensions (A549 epithelial cells, EA.hy926 endothelial cells, and MRC5 fibroblasts) were modified with 2.5% w/v PVP-based bio-inks according to a previous study^[70] and the printed output of respective cells were evaluated over a period of 30 min (0, 10, 20, and 30 min). To mimic the cell density within the native alveolar lung tissue, the A549 epithelial cells and EA.hy926 endothelial cells were printed at a cell density of 2 million cells/ml to create densely-packed cell layers, while the MRC5 fibroblasts were printed at a cell density of 0.75 million cells/ml to create sparsely distributed fibroblast layer. The modified PVP-based cell suspensions were loaded into printing cartridges and allowed to reach an equilibrium for 5 min before printing. The Biofactory® bioprinter (RegenHU, Switzerland) was used for cell printing studies; different microvalve-based printheads (100 and 300 µm diameter) were used to deposit cell droplets (15 arrays of 3 × 3 cell droplets) ($n = 135$) onto Corning® (Merck CLS430165) tissue-culture treated culture dishes (35 mm × 10 mm). The printed arrays of cell droplets were evaluated for its cell output/droplet and initial printed cell viability using Live/Dead Viability/Cytotoxicity kits (Invitrogen™ L3224, Thermo Fisher Scientific). For the long-term proliferation study, the printed arrays of cell droplets were immediately cultured with the co-culture medium inside an incubator at 37°C and 5% CO₂ over a period of 7 days. The PrestoBlue® assay (Invitrogen™ A13262, Thermo Fisher Scientific) was used to measure the proliferation profile for both printed and non-printed cells (control)

based on the normalized relative fluorescence units over a period of 7 days (day 1, 4, and 7) post-printing.

(2) Bioprinting of 3D triple-layered human alveolar lung models

The 3D triple-layered human alveolar lung model consisted of A549 human lung epithelial cells (top), EA.hy926 human endothelial cells (middle) and MRC-5 human lung fibroblasts (bottom). The sequence of printing was as follows: Collagen >MRC-5 >EA.hy926 >Collagen >A549 (CMECA) to mimic the spatial arrangement of native lung alveolar cells and its ECM. The Biofactory® bioprinter (with up to 8 different customizable printheads) was used to fabricate the 3D triple-layered human alveolar lung models, with multiple microvalve-based printheads (100 µm and 300 µm diameter nozzles) for collagen and cell printing, respectively. A collagen layer was first fabricated by printing discrete droplets of cold collagen precursor solution (Type I rat tail, 3.68 mg/ml from corning) along adjacent lines, at a fixed spacing of 0.8 mm and a droplet dispensing frequency of 55.6 Hz and 800 mm/min, onto the membrane of a Transwell insert (1 µm pore size, corning). This was then cross-linked by printing discrete sodium bicarbonate solution droplets (NaHCO₃ – a mild alkaline buffer solution at 0.8 M) at 2 mm spacing directly below and above the collagen layer, following our published protocol^[71]. Next, MRC5 lung fibroblasts (0.75 mil cells/ml) were deposited onto the crosslinked collagen layer at 2 mm spacing (3 drops per spot) to create sparsely distributed fibroblast layer. The collagen-MRC5 constructs were then incubated overnight in culture medium. On the next day, discrete droplets of EA.hy926 endothelial cells (2 mil cells/ml) were printed over the elongated MRC5 fibroblast layer at 1 mm spacing (5 drops per spot). The printed cells were incubated for 60 min to allow sedimentation and attachment to the bottom cell layers. This is to help mitigate cell dislodgement during subsequent printing operation. Following that, a collagen layer was printed using the same approach as described earlier. Finally, discrete droplets of A549 epithelial cells (2 mil cells/ml) were printed over the collagen layer at 1 mm spacing (5 drops per spot) and incubated for 60 min before addition of culture medium. The 3D bioprinted human alveolar lung models were cultivated in a humid incubator under liquid-liquid interface (LLI – submerged condition) for 3 days, before further maturation at air-liquid interface (ALI) for up to an additional 11 days (4, 7 or 11 days of ALI).

2.3. Characterization of the 3D triple-layered human alveolar lung models

(1) Survivability post-printing

The Live-or-Dye NucFix™ Red (Biotium, CA, USA) fluorescence dye stains dead cells at the nucleus and has an absorption/emission maximum intensity at

520/593 nm, which can be viewed with a PE-Texas red filter. The procedure was performed according to the supplier's instruction. Briefly, a 1000× stock of Live-or-Dye was initially prepared by dissolving the dye with 50 µl of anhydrous DMSO, then aliquoted and kept in a -20°C freezer. The 3D tissue construct's cell culture medium was removed, and the cells rinsed thoroughly using 1× PBS to minimize background signal. The cells were stained with a 0.1× Live-or-Dye working solution in PBS at room temperature for 30 min, followed by washing twice with PBS (5 min per wash), and fixation with cold acetone (stored in -20°C freezer) for 10 min. Fixed cells were then washed thrice with PBS, with DAPI (4',6-Diamidino-2-phenylindole dihydrochloride, Sigma) nuclear counterstain added to the PBS in the first wash. After washing, the membrane from the Transwell insert was removed, placed onto glass slides, and cover slipped using ProLong™ Gold Antifade Mountant (Invitrogen) mounting medium. The samples were left to dry overnight before visualization using Olympus BX51 fluorescent microscope. Representative fluorescence images were captured; the number of dead cells stained positively by Live-or-Dye and the total number of cells stained by DAPI was counted using ImageJ Fiji image analysis software, to determine the long-term survivability (7, 10, and 14 days) of the 3D bioprinted human alveolar lung models.

(2) Immunofluorescence staining

For immunofluorescence staining, the 3D tissue constructs were fixed using cold acetone for 10 min before performing cell permeabilization for 10 min with 0.1% Triton X-100 in PBS at room temperature. Rabbit anti-aquaporin-5 polyclonal antibody (Invitrogen Cat no: PA5-77710; dilution 1:400), rabbit anti-caveolin-1 polyclonal antibody (Boster Biological Technology Cat no: PA1514; dilution 1:400), rabbit anti-prosurfactant protein C (Pro-SPC) polyclonal antibody (Merck Cat no: AB3786; dilution 1:400), mouse anti-pan-Cytokeratin-FITC monoclonal antibody (GeneTex Cat no: GTX11212; dilution 1:500), and rabbit anti-CD31 polyclonal antibody (Abcam Cat no: AB32457; dilution 1:200) dissolved in 3% bovine serum albumin (BSA)/0.01% Triton X-100 PBS solution were then incubated with the fixed cells at 4°C overnight. After overnight incubation, the fixed cells were washed thrice with 1× PBS, at room temperature. Secondary anti-rabbit antibody labelled with Alexa Fluor 568 (Invitrogen Cat no: A10037; dilution 1:400) were dissolved in 3% BSA/0.01% Triton X-100 PBS solution and added to all samples, except anti-pan Cytokeratin-FITC, followed by incubation with gentle shaking in the dark for 2 h at room temperature. Finally, the cells were washed thrice with PBS, with DAPI nuclear counterstain added to the PBS in the first wash. The membrane from the Transwell insert was then removed, placed onto glass slides, and cover slipped using

ProLong™ Gold Antifade mounting medium. The samples were left to dry overnight before visualization using Olympus IX73 fluorescent microscope and Olympus FV-1000 confocal microscope, respectively.

2.4. Statistical analysis

All experimental results are presented as mean ± standard deviation. Statistical comparisons were performed using Student's *t*-test. Values are significantly different when $P < 0.01$. Significance levels are as follows: $P < 0.001$ (***) as the most significant and $P < 0.01$ (*) as the least significant.

3. Results and discussion

3.1. Influence of co-culture medium for human alveolar cells

Three different types of human alveolar lung cell lines were selected for this study and they were A549 epithelial cells (grown in RPMI-1640 culture medium), EA.hy926 endothelial cells (grown in DMEM/F12 culture medium), and MRC5 fibroblasts (grown in DMEM/F12 culture medium). These are common cell lines used in research laboratories as *in-vitro* disease models to study respiratory pathogen biology. Hence, we reasoned that these cell lines would be good representatives to construct the lung models in our study. Our first objective of the study was to select a co-culture medium which would enable the proliferation of all three different human lung cell lines in the 3D bio-printed form. This was achieved by measuring the proliferation rate of each of the three cell lines in different ratio composition of the original culture media prepared, RPMI-1640 and DMEM/F12 culture medium. The best ratio composition found suitable as the co-culture medium was found to be 1:1 v/v of RPMI-1640 to DMEM/F12 culture medium and the results are shown in **Figure 1**. The three different cell lines were cultured individually in 1:1 v/v of RPMI-1640 to DMEM/F12 culture medium (labeled as co-culture in **Figure 1(A)**) and their cell morphologies compared with their respective culture medium (labeled as control in **Figure 1(A)**). The adherent cells were stained with Live/Dead Viability/Cytotoxicity kits (Invitrogen™ L3224) for easy visualization with an inverted microscope system (IX53, Olympus, Japan) under 10× magnification. The live cells stained the typical green color while the dead cells stained the typical red color. The growth pattern for all three different human alveolar lung cells in both co-culture and control media was monitored on day 1, day 4, and day 7. The increase in number of stained cells was progressively observed from day 1 to day 7 which represented about 90% confluency between both media. In addition, the morphologies were also observed to be highly similar between both media (**Figure 1A**). Both

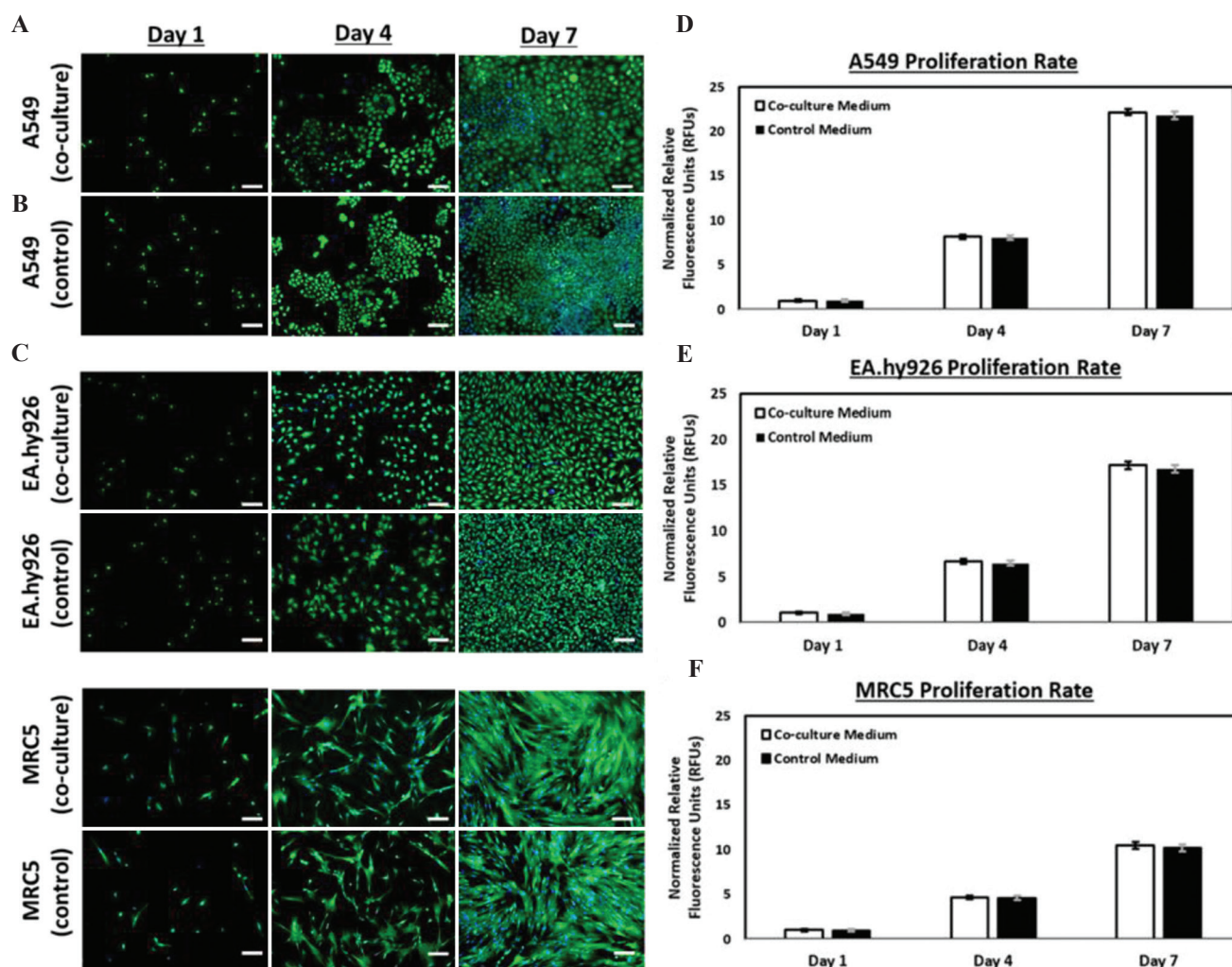


Figure 1. (Left) Representative fluorescence images of (A) A549 human lung epithelial cells, (B) EA.hy926 human endothelial cells, and (C) MRC-5 human lung fibroblasts (bottom), cultured in different culture medium (co-culture medium and control medium – A549 with RPMI-1640 culture medium supplemented with 10% fetal bovine serum [FBS] and both EA.hy926 and MRC-5 with DMEM/F12 culture medium supplemented with 10% FBS) over a period of 7 days – the green fluorescent represents the viable cells while the blue fluorescent represent the cell nuclei; scale bar: 100 μ m. (Right) Influence of co-culture medium on proliferation profile of (D) A549 human lung epithelial cells, (E) EA.hy926 human endothelial cells, and (F) MRC-5 human lung fibroblasts over a period of 7 days.

the A549 and EA.hy926 cells exhibited the cobblestone morphology, while the MRC5 fibroblasts exhibited the elongated morphology. Next, the proliferation rates of all three human cell lines were measured using normalized relative fluorescence units from the PrestoBlue[®] assay. As observed, the proliferation rates of all three human cell lines were observed to be relatively similar in the co-culture (indicated as white bar) and original growth media (indicated as black bar) (Figure 1B and 1C). The proliferation assay was not evaluated further after 7 days as the cells would overgrow and start aging, and this would not be able to provide any meaningful or additional information. Taken together, our findings on the cell morphology and proliferation rate showed that the ratio composition of 1:1 v/v of RPMI-1640 to DMEM/F12

culture medium is suitable as a co-culture medium and this composition was used for the whole study.

3.2. Optimization of cell printing parameters

The next critical step was to evaluate and determine the printed cell output for consistent and scalable fabrication of 3D bioprinted human alveolar lung models. A 30-min printing window is considered reasonably long for printing of multiple 3D tissue constructs due to the high-throughput rates for the jetting-based bioprinting technique. To mimic the cell density within the native alveolar lung tissue, the A549 epithelial cells and EA.hy926 endothelial cells were printed at a cell density of 2 million cells/ml to create densely-packed cell layers while the MRC5 fibroblasts were printed at a cell density

of 0.75 million cells/ml to create a sparsely distributed fibroblast layer. Notably, the MRC5 fibroblasts utilized in this study were observed to form large cell clumps over time and this led to the clogging of printhead with a nozzle diameter of 100 μm after 25 min of cell printing. The clogging issue for the MRC5 fibroblasts can be mitigated by using a larger nozzle diameter of 300 μm and this was used to print the different human alveolar lung cells for all subsequent experiments in this study.

The modified PVP-based cell suspensions are first loaded into printing cartridges and allowed to reach an equilibrium for 5 min before printing. The printed cell output per droplet for A549 epithelial cells (2×10^6 cells/ml) showed small fluctuation from 59.7 ± 5.1 cells per droplet at 0-min interval to 60.8 ± 5.3 cells per droplet at 30-min interval. For

the EA.hy926 endothelial cells (2×10^6 cells/ml), the printed cell output per droplet showed small fluctuations from 62.5 ± 5.6 cells per droplet at 0-min interval to 64.1 ± 4.8 cells per droplet at 30-min interval. The printed cell output per droplet for MRC5 fibroblasts (0.75×10^6 cells/ml) also shows negligible fluctuation from 18.4 ± 5.9 cells per droplet at 0-min interval to 19.1 ± 4.4 cells per droplet at 30-min interval. Hence, the use of 2.5% w/v PVP-modified cell suspension and a larger nozzle diameter of 300 μm facilitates the printing of different human alveolar lung cells (A549 epithelial cells, EA.hy926 endothelial cells, and MRC5 fibroblasts) with high consistency over a period of 30 min (**Figure 2A and B**).

Next, the initial viability of the printed cells is compared against the control non-printed cells. The Molecular Probes® Live/Dead staining kit stains the

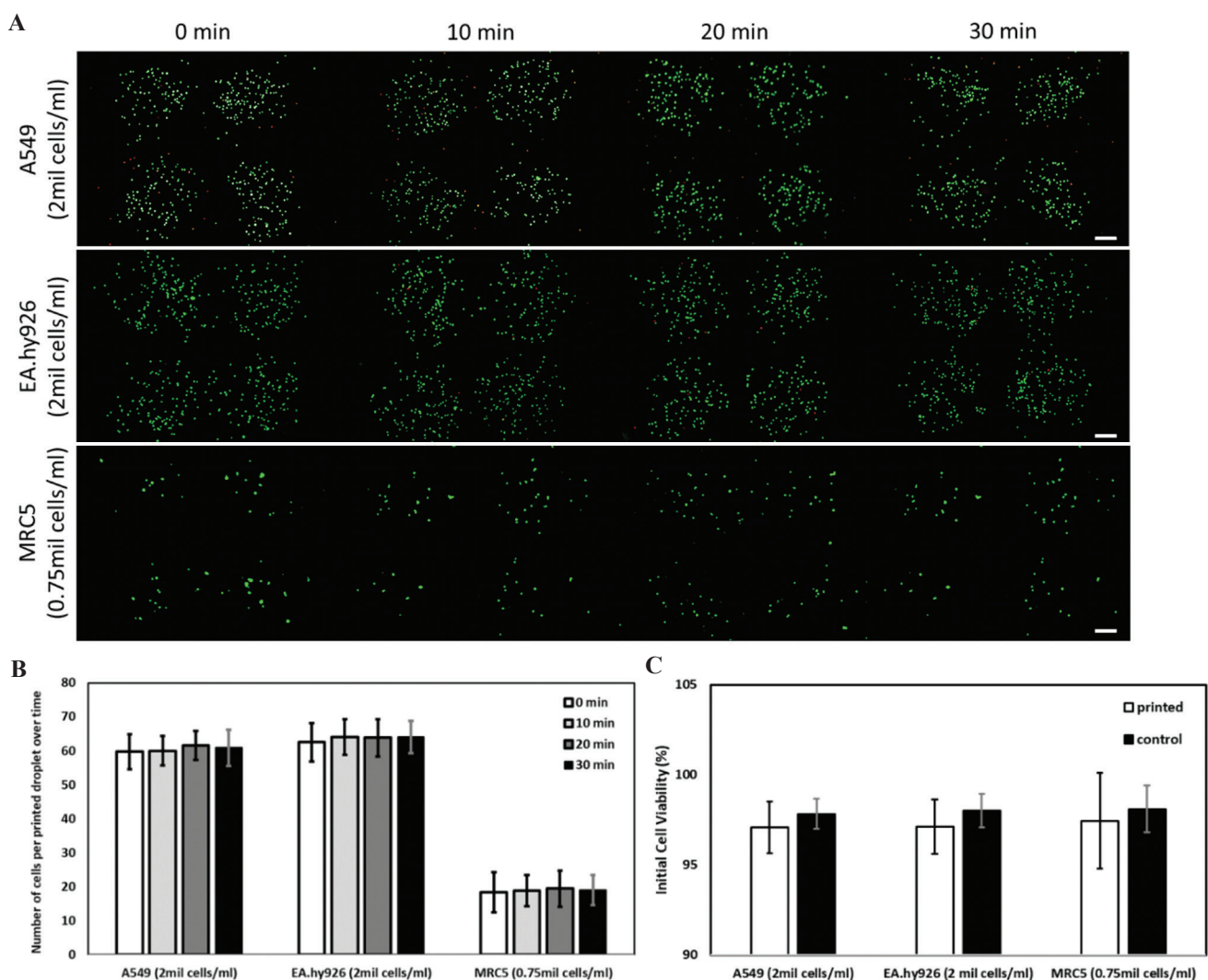


Figure 2. (A) Representative Molecular Probes® Live/Dead stained fluorescence images of different types of printed human alveolar lung cells: A549 human lung epithelial cells (top), EA.hy926 human endothelial cells (middle) and MRC-5 human lung fibroblasts (bottom) at varying cell concentrations at different time intervals (0, 10, 20, and 30-min intervals); scale bar: 200 μm . (B) Analysis of number of printed cells per droplet over a period of 30 min (average \pm standard deviation). (C) Influence of printing process on initial cell viability (Live/Dead staining kit) – printed cells versus non-printed cells (control).

viable cells green and the dead cells red. The initial cell viability of printed cells (A549, EA.hy926, and MRC5) is as follows: $97.1 \pm 1.4\%$, $97.1 \pm 1.5\%$, and $97.4 \pm 2.6\%$, respectively, while the initial cell viability of control non-printed cells (A549, EA.hy926, and MRC5) is as follows: $97.8 \pm 0.8\%$, $98.0 \pm 0.9\%$, and $98.0 \pm 1.3\%$ (**Figure 2C**). Hence, the printing process has no significant effect on the printed cells as compared to the control non-printed cells.

Further study was performed to evaluate the influence of printing process on the long-term viability of the printed cells (A549, EA.hy926, and MRC5) over time (day 1, 4, and 7) using Molecular Probes® Live/Dead staining for fluorescence imaging and PrestoBlue cell proliferation assay for quantitative measurement.

The number of viable cells at any given time point can be measured and expressed in terms of relative fluorescent units (RFUs) from the fluorescence readout. The RFUs are normalized with respect to day 1 for each type of cells (both printed and non-printed) for easy comparison of long-term viability across different groups. In general, the normalized RFUs for the printed cells are relatively similar to those control non-printed cells at different time intervals (day 1, 4, and 7). The proliferation profile of both printed and control non-printed cells follows similar trend as the earlier experiment on co-culture medium, whereby the proliferation rate of the three different human alveolar lung cells is as follows: A549 >EA.hy926 >MRC5 (**Figure 3**). Furthermore, the deposition of cell-

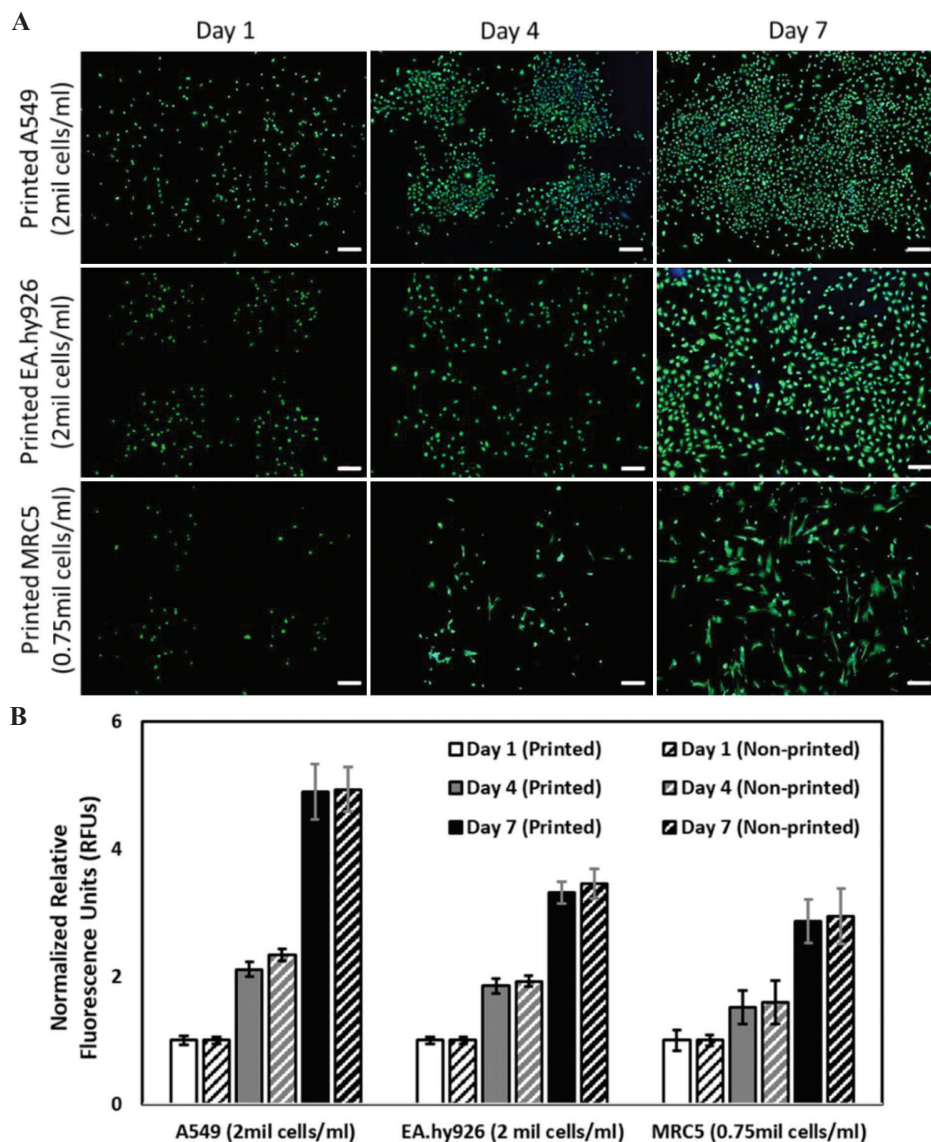


Figure 3. (A) Representative Molecular Probes® Live/Dead stained fluorescence images of different types of printed human alveolar cells: A549 human lung epithelial cells (top), EA.hy926 human endothelial cells (middle), and MRC-5 human lung fibroblasts (bottom) at varying cell concentrations, at different time points post-printing (day 1, 4, and 7); scale bar: 200 μ m. (B) Proliferation profile of printed and non-printed (control) human alveolar cells over a period of 7 days.

laden droplets using DOD bioprinting technique enables the cells to proliferate and spread uniformly to form a homogeneous cell layer at day 7. As the printed cells were close to 90% confluence by day 7 for both A549 and EA.hy926, further proliferation studies for all 3 types of cells were not continued. As such, we have demonstrated the use of microvalve-based bioprinting technique can achieve consistent printed cell output with high short-term (>97%) and long-term viability (over a period of at least 7 days) using the PVP-modified cell suspension. This is critical for 3D DOD bioprinting of different human alveolar lung cells to achieve precise and uniform cell deposition and patterning within the 3D tissue constructs to achieve high repeatability at high-throughput rates.

3.3. Characterization of 3D bioprinted triple-layered human alveolar lung models

(A) Long-term survivability

The 3D triple-layered human alveolar lung model consisted of A549 human lung epithelial cells (top), EA.hy926 human endothelial cells (middle), and MRC-5 human lung fibroblasts (bottom). The sequence of printing was as follows: Collagen >MRC-5 >EA.hy926 >Collagen >A549 (CMECA) to mimic the spatial arrangement of native lung alveolar cells and its ECM (**Figure 4A**). The

A549 epithelial cells cultured under submerged condition exhibited clear cell edges and organelles and covered more than 70% surface of the 3D alveolar lung tissue models after 3 days of culture under LLI condition. Conversely, the A549 epithelial cells cultured under ALI condition started to flatten and formed compacted layer initially before forming some spheroid-like structures on top of the flattened cell layer over time. The observations from our work are corroborated by other studies that characterized the mono-culture of A549 cells at ALI interface^[72,73].

In general, the 3D bioprinted alveolar lung models show high viability (>96%) over a period of 14 days. It is noted that the overall viability of the 3D bioprinted human alveolar lung models is higher at day 10 and 14 as compared to day 7; this is likely due to cell proliferation over time that led to an increase in the total number of cells, resulting in a lower ratio of dead cells to total number of cells (**Figure 4B**).

(2) Immunofluorescence staining analysis

To determine the influence of culture conditions (ALI vs. LLI conditions) on the maturation of 3D bioprinted human alveolar lung models, the lung tissue models were stained for the presence of alveolar type I (AT-1) biomarkers (aquaporin-5, caveolin-1), alveolar type II (AT-2) biomarker (Pro-SPC), epithelial biomarker (pan-

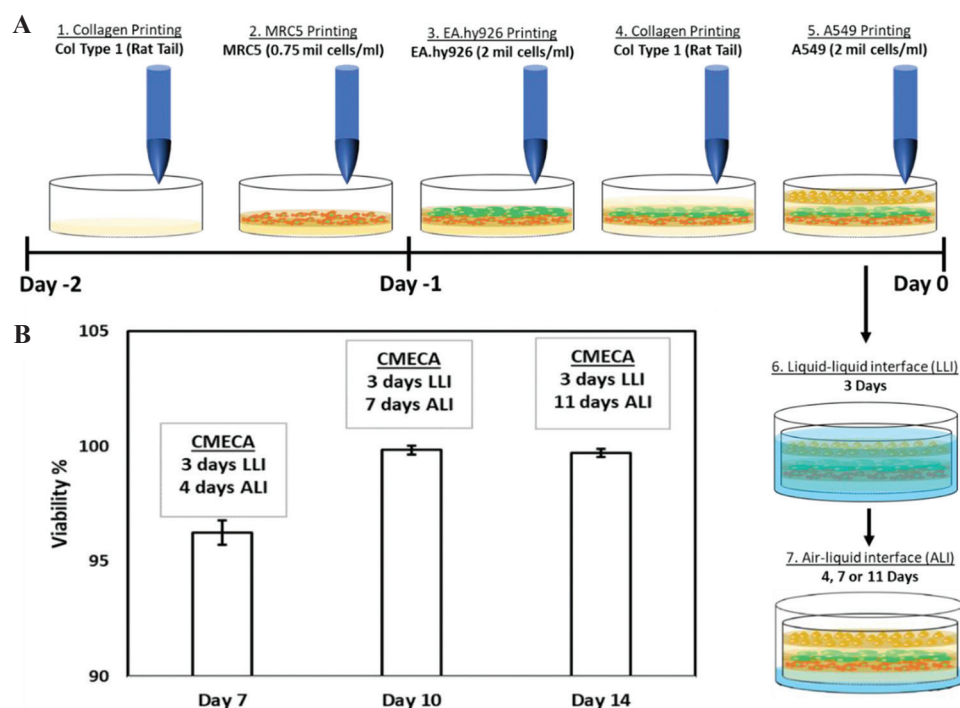


Figure 4. (A) Bioprinting process of the 3D triple-layered human alveolar lung models; the ECM bio-inks and cell droplets are deposited in the following order: Collagen >MRC-5 >EA.hy926 >Collagen >A549 to mimic the spatial arrangement of native alveolar blood-air lung cells from the basal to apical layers, and its ECM. The 3D bioprinted blood-air barrier models are then cultivated under liquid-liquid interface (submerged condition) for the first 3 days followed by air-liquid interface up to additional 11 days. (B) The graph shows the survivability results of the triple-layered blood-air barrier models (CMECA) over a culture period of 14 days based on NucFix staining.

cytokeratin), and endothelial biomarker (CD31 also known as PECAM-1). Here, we focused only on the staining of epithelial and endothelial layers as these two main layers are representative of the air-blood barrier. The AT2 cells can undergo trans-differentiation into type 1 alveolar epithelial cells (AT1)^[74] and hence, we checked for the presence of both AT-1 and AT-2 biomarkers in this study. We performed immunofluorescence analysis of the human alveolar lung models on day 7 as it is deemed to

be a reasonably long tissue maturation duration for the different alveolar lung cells to interact, proliferate, and differentiate based on prior works^[31,60,62-64].

From the immunostaining analysis (**Figure 5**), we observed the presence of all the biomarkers except for AT-1 biomarkers (aquaporin-5 and caveolin-1) in both groups of 3D bioprinted human alveolar lung models cultured under ALI and LLI conditions, respectively. It was reported in an earlier study that the A549 cells

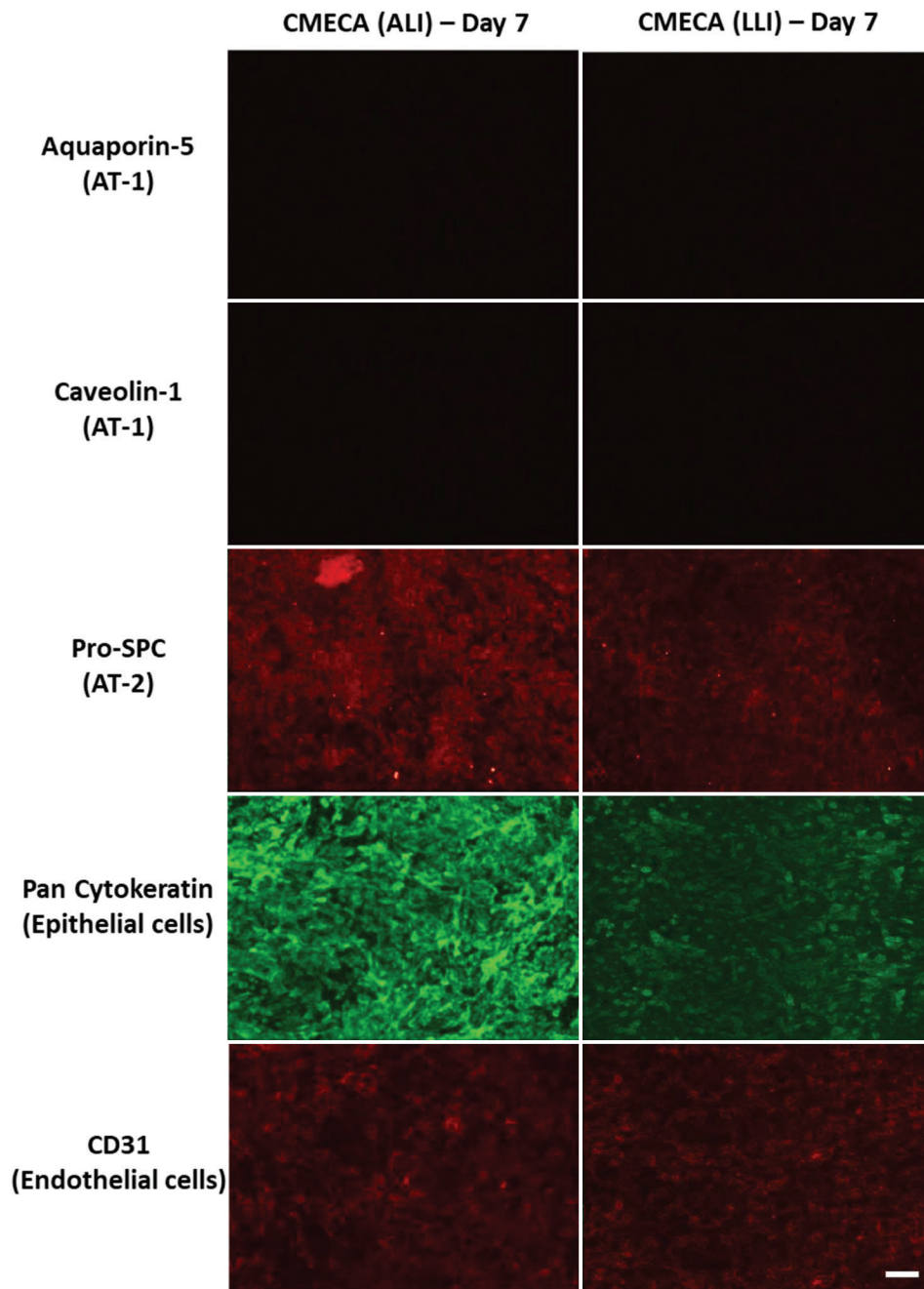


Figure 5. Immunostaining analysis of triple-layered blood-air barrier models (CMECA) cultured under ALI conditions (3 days LLI and 4 days ALI) and LLI conditions at day 7; scale bar: 200 μ m.

cultured under ALI condition expressed AT-1 biomarker (aquaporin-5)^[72]. However, the alveolar type II A549 lung epithelial cells in the 3D bioprinted human alveolar lung

models did not express the AT-1 biomarkers at day 7 as confirmed by the aquaporin-5 and caveolin-1 staining results. There is no significant difference between the

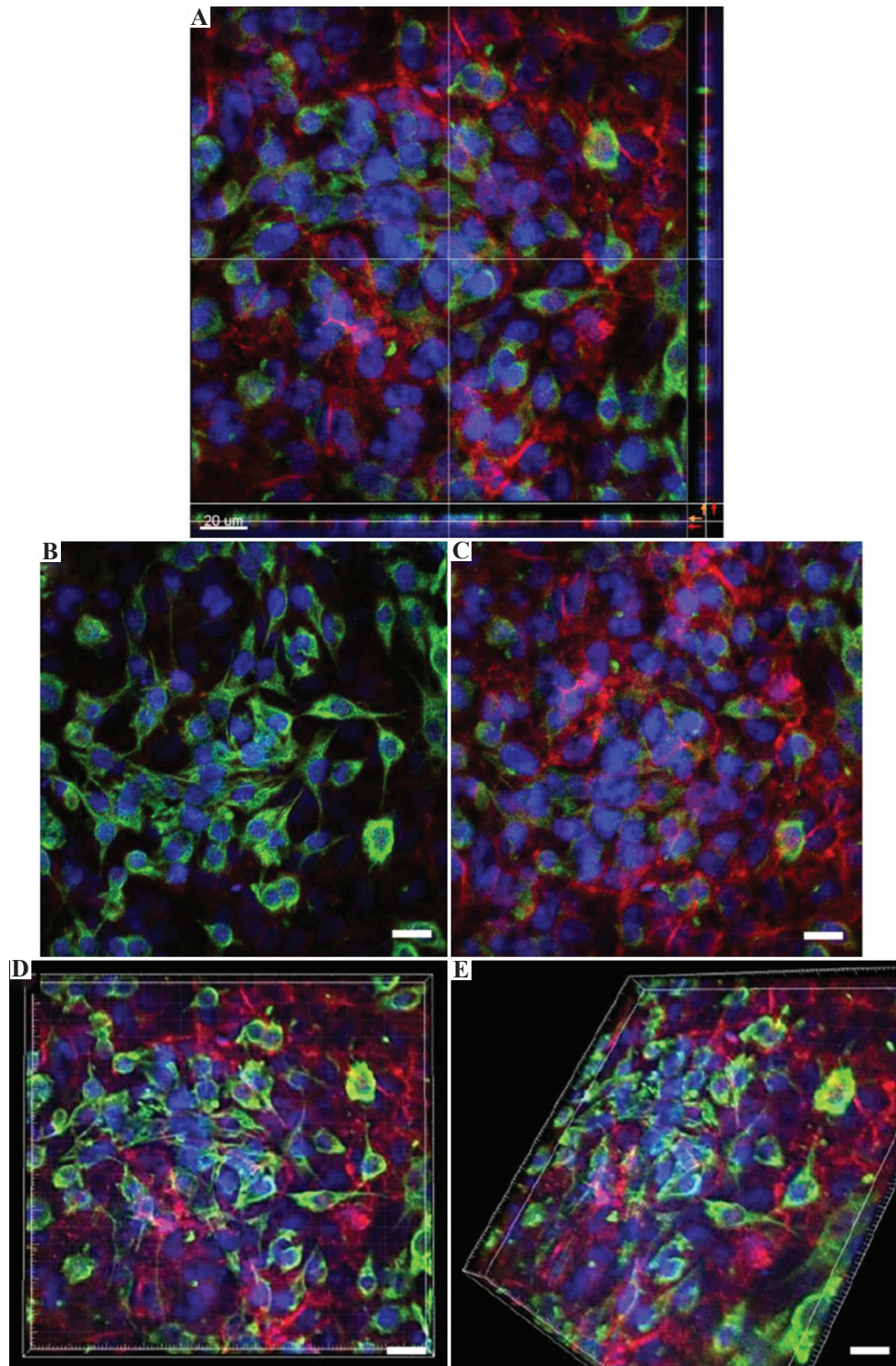


Figure 6. (A) Confocal imaging of 3D bioprinted human blood-air barrier model at day 14 using 60× magnification. (B) Representative image of a distinct upper layer of A549 epithelial cells – green and blue fluorescence; scale bar: 20 µm. (C) Representative image of a distinct lower layer of EA.hy926 endothelial cells – red and blue fluorescence (nuclear DNA); scale bar: 20 µm. (D, E). Representative composite images comprising upper layer of A549 epithelial cells and lower layer of EA.hy926 endothelial cells from top and rotated view, respectively; scale bar: 20 µm.

expression of CD31 biomarker (endothelial cells) in both ALI and LLI culture conditions, as the EA.hy926 endothelial cells are embedded within the 3D bioprinted human alveolar lung models. It is observed that there is an increased in fluorescence signals from pro-SPC (AT-2) and pan-cytokeratin (epithelial cells) biomarkers for 3D bioprinted human alveolar lung models under the ALI culture condition at day 7 as compared to the LLI culture condition, suggesting an increased expression of the proteins. The ALI culture condition mimics the native environment of the blood-air barrier; hence, it is likely to result in an increased expression of pro-SPC (AT-2) and pan-cytokeratin (epithelial cells) biomarkers.

(3) Confocal imaging

To evaluate the cell distribution and thickness of the blood-air barrier models, confocal fluorescence imaging was performed at day 14 using 60× magnification for clear visualization of different types of alveolar lung cells within the 3D bioprinted human alveolar lung models. Here, we focused only on the staining of epithelial and endothelial layers as these two main layers are representative of the air-blood barrier. Multiple 3D bioprinted human alveolar lung models were used for confocal fluorescence imaging to image all the alveolar lung cells (red – CD31, a marker for endothelial cells, green – pancytokeratin, a marker for epithelial cells, and blue for cell nuclei); resulting in distinct layers of uppermost A549 epithelial lung cells with DAPI at slice 18 of confocal microscopy (stained in green and blue – **Figure 6B**) and bottom layer of EA.hy926 endothelial cells with DAPI at slice 27 of confocal microscopy (stained in red and blue – **Figure 6C**). Tiny random patches of missing epithelial cells could be observed at high magnification of 60× on this upper A549 cell layer (covering $79.4 \pm 12.5\%$ of epithelial surface) in the 3D bioprinted human alveolar lung models and the presence of “patchy” epithelial cell layer was also observed in other study using monolayer of A549 cells^[7].

The manually seeded *in-vitro* 3D lung tissue models in other published works measure $\sim 26 - 35 \mu\text{m}^{[31,60,61]}$, while the 3D bioprinted *in-vitro* 3D lung tissue models in an earlier published work measure $\sim 22 \mu\text{m}^{[31]}$. In comparison, the overall thickness of 3D bioprinted human alveolar lung models in this study was measured to be approximately 8 – 10 μm using confocal microscopy (**Figure 6A**).

4. Conclusion

This work successfully demonstrated the fabrication of 3D bioprinted triple-layered human alveolar lung models comprising of A549 human lung epithelial cells, EA.hy926 human endothelial cells, and MRC-5 human lung fibroblasts. The cell suspension was modified using 2.5% w/v PVP-based bio-inks for DOD bioprinting

process and printed through a suitable nozzle diameter of 300 μm to mitigate nozzle clogging. The use of PVP-based bio-inks led to a homogeneous and consistent cell output for the different types of human alveolar lung cells by achieving a neutral buoyancy state. The bioprinted cells showed high initial cell viability and proliferation profile similar to the control non-printed cells. The analysis of 3D bioprinted triple-layered human alveolar lung models confirmed the presence of Pro-SPC (AT-2), pan cytokeratin (epithelial lung cells), and CD31 (endothelial cells), suggesting that the cell types retained their functionalities when bio-printed. The ALI culture condition may lead to an increased expression of pro-SPC (AT-2) and pan-cytokeratin (epithelial cells) biomarkers for 3D bioprinted lung models on day 7, as compared to the LLI culture condition. The use of DOD bioprinting techniques facilitated precise spatial positioning of the different types of human alveolar lung cells to form distinct cell layers within the 3D bioprinted lung tissue models. Furthermore, the 3D bioprinted alveolar lung tissue models showed high survivability rates over a long-term period of at least 14 days. The *in-vitro* 3D lung models established using these three cell lines demonstrated the consistency and repeatability of 3D bioprinting systems. Future studies can be extended with the use of primary human alveolar cells for pathogen translocation studies and respiratory-related toxicological testing applications. Collectively, we have demonstrated a repeatable, scalable, and high-throughput DOD bioprinting process in this work for the fabrication of triple-layered human alveolar lung models that can be cultured over a period of 14 days with high survivability rates. This would help to address the demand for highly repeatable and scalable fabrication of 3D *in-vitro* alveolar lung models using 3D bioprinting techniques.

Compliance with ethics guidelines

This study does not contain any studies with human or animal subjects performed by any of the authors.

Acknowledgements

We thanked DSO National Laboratories for sponsoring this project and NTU SC3DP for the use of equipment.

Conflicts of interest

All authors declare that they have no conflicts of interest.

References

1. Wu Z, McGoogan JM, 2019, Characteristics of and Important Lessons from the Coronavirus Disease 2019 (COVID-19) Outbreak in China: Summary of a Report of 72 314 Cases

- from the Chinese Center for Disease Control and Prevention. *JAMA*, 323:1239–42.
<https://doi.org/10.1001/jama.2020.2648>
2. Oboho IK, Tomczyk SM, Al-Asmari AM, *et al.*, 2015. 2014 MERS-CoV Outbreak in Jeddah a Link to Health Care Facilities. *N Engl J Med*, 372:846–54.
<https://doi.org/10.1056/nejmoa1408636>
 3. Bautista E, Chotpitayasunondh T, Gao Z, 2010, Influenza, Clinical Aspects of Pandemic 2009 Influenza A (H1N1) Virus Infection. *N Engl J Med*, 362:1708–19.
<https://doi.org/10.1056/nejmra1000449>
 4. Seto W, Tsang D, Yung RW, *et al.*, 2003. Effectiveness of Precautions against Droplets and Contact in Prevention of Nosocomial Transmission of Severe Acute Respiratory Syndrome (SARS). *Lancet*, 361:1519–20.
[https://doi.org/10.1016/s0140-6736\(03\)13168-6](https://doi.org/10.1016/s0140-6736(03)13168-6)
 5. Steimer A, Haltner E, Lehr CM, 2005, Cell Culture Models of the Respiratory Tract Relevant to Pulmonary Drug Delivery. *J Aerosol Med*, 18:137–82.
<https://doi.org/10.1089/jam.2005.18.137>
 6. Hermanns MI, Unger RE, Kehe K, *et al.*, 2004, Lung Epithelial Cell Lines in Coculture with Human Pulmonary Microvascular Endothelial Cells: Development of an Alveolo-Capillary Barrier *In Vitro*. *Lab Invest*, 84:736–52.
<https://doi.org/10.1038/labinvest.3700081>
 7. Nichols JE, Niles JA, Vega SP, *et al.*, 2014, Modeling the Lung: Design and Development of Tissue Engineered Macro- and Micro-physiologic Lung Models for Research Use. *Exp Biol Med*, 239:1135–69.
<https://doi.org/10.1177/1535370214536679>
 8. Ng WL, Chua CK, Shen YF, 2019, Print Me An Organ! Why We Are Not There Yet. *Prog Polym Sci*, 97:101145.
<https://doi.org/10.1016/j.progpolymsci.2019.101145>
 9. Sun W, Starly B, Daly AC, *et al.*, 2020, The Bioprinting Roadmap. *Biofabrication*, 12:022002.
 10. Ng WL, Chan A, Ong YS, *et al.*, 2020, Deep Learning for Fabrication and Maturation of 3D Bioprinted Tissues and Organs. *Virtual Phys Prototyp*, 15:340–58.
 11. Zhang B, Gao L, Ma L, *et al.*, 2019, 3D Bioprinting: A Novel Avenue for Manufacturing Tissues and Organs. *Engineering*, 5:777–94.
<https://doi.org/10.1016/j.eng.2019.03.009>
 12. Ren KF, Hu M, Zhang H, *et al.*, 2019, Layer-by-Layer Assembly as a Robust Method to Construct Extracellular Matrix Mimic Surfaces to Modulate Cell Behavior. *Prog Polym Sci*, 92:1–34.
<https://doi.org/10.1016/j.progpolymsci.2019.02.004>
 13. Liu F, Liu C, Chen Q, *et al.*, 2018, Progress in Organ 3D Bioprinting. *Int J Bioprint*, 4:128–42.
 14. Ng WL, Lee JM, Zhou M, *et al.*, 2020, Hydrogels for 3-D bioprinting-based tissue engineering. In: R. Narayan, editor. *Rapid Prototyping of Biomaterials*, Elsevier, Chapel Hill, NC, pp. 183–204.
<https://doi.org/10.1016/b978-0-08-102663-2.00008-3>
 15. Lee JM, Suen SK, Ng WL, *et al.*, 2020, Bioprinting of Collagen: Considerations, Potentials, and Applications. *Macromol Biosci*, 21:2000280.
<https://doi.org/10.1002/mabi.202000280>
 16. Osidak EO, Kozhukhov VI, Osidak MS, *et al.*, 2020, Collagen as Bioink for Bioprinting: A Comprehensive Review. *Int J Bioprint*, 6:270.
<https://doi.org/10.18063/ijb.v6i3.270>
 17. Lee JM, Ng WL, Yeong WY, 2019, Resolution and Shape in Bioprinting: Strategizing Towards Complex Tissue and Organ Printing. *Appl Phys Rev*, 6:011307.
<https://doi.org/10.1063/1.5053909>
 18. Mir TA, Iwanaga S, Kurooka T, *et al.*, 2019, Biofabrication Offers Future Hope for Tackling Various Obstacles and Challenges in Tissue Engineering and Regenerative Medicine: A Perspective. *Int J Bioprint*, 5:153–63.
<https://doi.org/10.18063/ijb.v5i1.153>
 19. Kang HW, Lee SJ, Ko IK, *et al.*, 2016, A 3D Bioprinting System to Produce Human-Scale Tissue Constructs with Structural Integrity. *Nat Biotechnol*, 34:312–9.
<https://doi.org/10.1038/nbt.3413>
 20. Kim W, Kim G, 2019, Collagen/Bioceramic-based Composite Bioink to Fabricate a Porous 3D hASCs-laden Structure for Bone Tissue Regeneration. *Biofabrication*, 12:015007.
<https://doi.org/10.1088/1758-5090/ab436d>
 21. Ahlfeld T, *et al.*, 2018, Bioprinting of Mineralized Constructs Utilizing Multichannel Plotting of a Self-setting Calcium Phosphate Cement and a Cell-laden Bioink. *Biofabrication*, 10:045002.
<https://doi.org/10.1088/1758-5090/aad36d>
 22. Noor N, Shapira A, Edri R, *et al.*, 2019, 3D Printing of Personalized Thick and Perfusable Cardiac Patches and Hearts. *Adv Sci*, 6:1900344.
<https://doi.org/10.1002/advs.201900344>
 23. Jang J, Park HJ, Kim SW, *et al.*, 2017, 3D Printed Complex Tissue Construct Using Stem Cell-laden Decellularized Extracellular Matrix Bioinks for Cardiac Repair. *Biomaterials*, 112:264–74.
<https://doi.org/10.1016/j.biomaterials.2016.10.026>
 24. Izadifar M, Chapman D, Babyn P, *et al.*, 2018, UV-assisted

- 3D Bioprinting of Nanoreinforced Hybrid Cardiac Patch for Myocardial Tissue Engineering. *Tissue Eng Part C Methods*, 24:74–88.
<https://doi.org/10.1089/ten.tec.2017.0346>
25. You F, Chen X, Cooper D, et al., 2018, Homogeneous Hydroxyapatite/Alginate Composite Hydrogel Promotes Calcified Cartilage Matrix Deposition with Potential for Three-dimensional Bioprinting. *Biofabrication*, 11:015015.
<https://doi.org/10.1088/1758-5090/aaf44a>
 26. Nguyen D, Hägg D, Forsman A, et al., 2017, Cartilage Tissue Engineering by the 3D Bioprinting of iPSCs in a Nanocellulose/Alginate Bioink. *Sci Rep*, 7:658.
<https://doi.org/10.1038/s41598-017-00690-y>
 27. Izadifar Z, Chang T, Kulyk W, et al., 2016, Analyzing Biological Performance of 3D-Printed, Cell-impregnated Hybrid Constructs for Cartilage Tissue Engineering. *Tissue Eng Part C Methods*, 22:173–88.
<https://doi.org/10.1089/ten.tec.2015.0307>
 28. Norona LM, Nguyen DG, Gerber DA, et al., 2019, Bioprinted Liver Provides Early Insight into the Role of Kupffer Cells in TGF- β 1 and Methotrexate-induced Fibrogenesis. *PLoS One*, 14:e0208958.
<https://doi.org/10.1371/journal.pone.0208958>
 29. Nguyen DG, Funk J, Robbins JB, et al., 2016, Bioprinted 3D Primary Liver Tissues Allow Assessment of Organ-level Response to Clinical Drug Induced Toxicity *In Vitro*. *PLoS One*, 11:e0158674.
<https://doi.org/10.1371/journal.pone.0158674>
 30. Mazzocchi A, Devarasetty M, Huntwork R, et al., 2018, Optimization of Collagen Type I-hyaluronan Hybrid Bioink for 3D Bioprinted Liver Microenvironments. *Biofabrication*, 11:015003.
<https://doi.org/10.1088/1758-5090/aae543>
 31. Horváth L, Umehara Y, Jud C, et al., 2015, Engineering an *In Vitro* Air-blood Barrier by 3D Bioprinting. *Sci Rep*, 5:7974
<https://doi.org/10.1038/srep07974>
 32. Park JY, Ryu H, Lee B, et al., Development of a Functional Airway-on-a-chip by 3D Cell Printing. *Biofabrication*, 11:015002.
 33. Ng WL, Wang S, Yeong WY, et al., 2016, Skin Bioprinting: Impending Reality or Fantasy? *Trends Biotechnol*, 34:689–99.
<https://doi.org/10.1016/j.tibtech.2016.08.009>
 34. Cubo N, Garcia M, del Cañizo JE, et al., 2016, 3D Bioprinting of Functional Human Skin: Production and *In Vivo* Analysis. *Biofabrication*, 9:015006.
<https://doi.org/10.1088/1758-5090/9/1/015006>
 35. Kim BS, Lee JS, Gao G, et al., 2017, Direct 3D Cell-printing of Human Skin with Functional Transwell System. *Biofabrication*, 9:025034.
<https://doi.org/10.1088/1758-5090/aa71c8>
 36. Ng WL, Tan ZQ, Yeong WY, et al., 2018, Proof-of-concept: 3D Bioprinting of Pigmented Human Skin Constructs. *Biofabrication*, 10:025005.
<https://doi.org/10.1088/1758-5090/aa9e1e>
 37. Ng WL, Yeong WY, 2019, The Future of Skin Toxicology Testing 3D Bioprinting Meets Microfluidics. *Int J Bioprint*, 5:237.
<https://doi.org/10.18063/ijb.v5i2.1.237>
 38. Kathawala MH, Ng WL, Liu D, et al., 2019, Healing of Chronic Wounds an Update of Recent Developments and Future Possibilities. *Tissue Eng Part B Rev*, 25:429–44.
<https://doi.org/10.1089/ten.teb.2019.0019>
 39. Zhuang P, Ng WL, An J, et al., 2019, Layer-by-layer Ultraviolet Assisted Extrusion-Based (UAE) Bioprinting of Hydrogel Constructs with High Aspect Ratio for Soft Tissue Engineering Applications. *PLoS One*, 14:e0216776.
<https://doi.org/10.1371/journal.pone.0216776>
 40. Ozbolat IT, Hospodiuk M, 2016, Current Advances and Future Perspectives in Extrusion-based Bioprinting. *Biomaterials*, 76:321–43.
<https://doi.org/10.1016/j.biomaterials.2015.10.076>
 41. Ng WL, Yeong WY, Naing MW, 2016, Development of Polyelectrolyte Chitosan-gelatin Hydrogels for Skin Bioprinting. *Procedia CIRP*, 49:105–12.
<https://doi.org/10.1016/j.procir.2015.09.002>
 42. Ng WL, Yeong WY, Naing MW, 2016, Polyelectrolyte Gelatin-chitosan Hydrogel Optimized for 3D Bioprinting in Skin Tissue Engineering. *Int J Bioprint*, 2:53–62.
<https://doi.org/10.18063/ijb.2016.01.009>
 43. Ng WL, Yeong WY, Naing MW, 2014, Potential of Bioprinted Films for Skin Tissue Engineering. Proceedings of the 1st International Conference on Progress in Additive Manufacturing, pp. 441–6.
https://doi.org/10.3850/978-981-09-0446-3_065
 44. Gudupati H, Dey M, Ozbolat I, 2016, A Comprehensive Review on Droplet-based Bioprinting: Past, Present and Future. *Biomaterials*, 102:20–42.
<https://doi.org/10.1016/j.biomaterials.2016.06.012>
 45. Ng WL, Lee JM, Yeong WY, et al., 2017, Microvalve-based Bioprinting Process, Bio-inks and Applications. *Biomater Sci*, 5:632–47.
<https://doi.org/10.1039/c6bm00861e>
 46. Ng WL, Yeong WY, Naing MW, 2016, Microvalve Bioprinting of Cellular Droplets with High Resolution and

- Consistency. Proceedings of the International Conference on Progress in Additive Manufacturing, pp. 397–402.
47. Koch L, Deiwick A, Franke A, *et al.*, 2018, Laser Bioprinting of Human Induced Pluripotent Stem Cells the Effect of Printing and Biomaterials on Cell Survival, Pluripotency, and Differentiation. *Biofabrication*, 10:035005. <https://doi.org/10.1088/1758-5090/aab981>
 48. Ng WL, Lee JM, Zhou M, *et al.*, 2020, Vat Polymerization-based Bioprinting Process, Materials, Applications and Regulatory Challenges. *Biofabrication*, 12:022001. <https://doi.org/10.1088/1758-5090/ab6034>
 49. Kim SH, Yeon YK, Lee JM, *et al.*, 2018, Precisely Printable and Biocompatible Silk Fibroin Bioink for Digital Light Processing 3D Printing. *Nat Commun*, 9:1620. <https://doi.org/10.1038/s41467-018-04517-w>
 50. Mandt D, Gruber P, Markovic M, *et al.*, 2018, Fabrication of Biomimetic Placental Barrier Structures within a Microfluidic Device Utilizing Two-photon Polymerization. *Int J Bioprint*, 4:144–55. <https://doi.org/10.18063/ijb.v4i2.144>
 51. Lim KS, Levato R, Costa PF, *et al.*, 2018, Bio-resin for High Resolution Lithography-based Biofabrication of Complex Cell-laden Constructs. *Biofabrication*, 10:034101. <https://doi.org/10.1088/1758-5090/aac00c>
 52. Ito Y, Correll K, Schiel JA, *et al.*, Lung Fibroblasts Accelerate Wound Closure in Human Alveolar Epithelial Cells through Hepatocyte Growth Factor/c-Met Signaling. *Am J Physiol Lung Cell Mol Physiol*, 307:L94–105. <https://doi.org/10.1152/ajplung.00233.2013>
 53. Panganiban RA, Day RM, 2011, Hepatocyte Growth Factor in Lung Repair and Pulmonary Fibrosis. *Acta Pharmacol Sin*, 32:12–20. <https://doi.org/10.1038/aps.2010.90>
 54. Kanaji N, *et al.*, 2017, Hepatocyte Growth Factor Produced in Lung Fibroblasts Enhances Non-small Cell Lung Cancer Cell Survival and Tumor Progression. *Respir Res*, 18:118. <https://doi.org/10.1186/s12931-017-0604-z>
 55. Carterson A, *et al.*, 2005, A549 Lung Epithelial Cells Grown as Three-dimensional Aggregates: Alternative Tissue Culture Model for *Pseudomonas aeruginosa* Pathogenesis. *Infect Immun*, 73:1129–40. <https://doi.org/10.1128/iai.73.2.1129-1140.2005>
 56. Paczosa MK, Fisher ML, Maldonado-Arocho FJ, Mencias J, 2014, Yersinia Pseudotuberculosis Uses Ail and YadA to Circumvent Neutrophils by Directing Yop Translocation during Lung Infection. *Cell Microbiol*, 16:247–68. <https://doi.org/10.1111/cmi.12219>
 57. Davidson DJ, Dorin JR, McLachlan G, *et al.*, 1995, Lung Disease in the Cystic Fibrosis Mouse Exposed to Bacterial Pathogens. *Nat Genet*, 9:351–7. <https://doi.org/10.1038/ng0495-351>
 58. Essaidi-Laziosi M, Brito F, Benaoudia S, *et al.*, 2018, Propagation of Respiratory Viruses in Human Airway Epithelia Reveals Persistent Virus-specific Signatures. *J Allerg Clin Immunol*, 141:2074–84. <https://doi.org/10.1016/j.jaci.2017.07.018>
 59. Weibel ER, 2015, On the Tricks Alveolar Epithelial Cells Play to Make a Good Lung. *Am J Respir Crit Care Med*, 191:504–13. <https://doi.org/10.1164/rccm.201409-1663oe>
 60. Costa A, de Souza Carvalho-Wodarz C, Seabra V, *et al.*, 2019, Triple co-culture of Human Alveolar Epithelium, Endothelium and Macrophages for Studying the Interaction of Nanocarriers with the Air-blood Barrier. *Acta Biomater*, 91:235–47. <https://doi.org/10.1016/j.actbio.2019.04.037>
 61. Klein SG, Serchi T, Hoffmann L, Blömeke B, *et al.*, 2013, An Improved 3D Tetraculture System Mimicking the Cellular Organisation at the Alveolar Barrier to Study the Potential Toxic Effects of Particles on the Lung. *Part Fibre Toxicol*, 10:31. <https://doi.org/10.1186/1743-8977-10-31>
 62. Bengalli R, Mantecca P, Camatini M, *et al.*, 2012, Effect of Nanoparticles and Environmental Particles on a Cocultures Model of the Air-blood Barrier. *BioMed Res Int*, 2013:801214. <https://doi.org/10.1155/2013/801214>
 63. Short KR, *et al.*, 2016, Influenza Virus Damages the Alveolar Barrier by Disrupting Epithelial Cell Tight Junctions. *Eur Respir J*, 47:954–66.
 64. Dekali S, Gamez C, Kortulewski T, *et al.*, 2014, Assessment of an *In Vitro* Model of Pulmonary Barrier to Study the Translocation of Nanoparticles. *Toxicol Rep*, 1:157–71. <https://doi.org/10.1016/j.toxrep.2014.03.003>
 65. Wang G, Zhang X, Liu X, *et al.*, 2019, Ambient Fine Particulate Matter Induce Toxicity in Lung Epithelial-endothelial Co-culture Models. *Toxicol Lett*, 301:133–45. <https://doi.org/10.1016/j.toxlet.2018.11.010>
 66. Alfaro-Moreno E, Nawrot TS, Vanaudenaerde BM, *et al.*, 2008, Co-cultures of Multiple Cell Types Mimic Pulmonary Cell Communication in Response to Urban PM10. *Eur Respir J*, 32:1184–94. <https://doi.org/10.1183/09031936.00044008>
 67. Herzog F, Clift MJ, Piccapietra F, *et al.*, 2013, Exposure of Silver-nanoparticles and Silver-ions to Lung Cells *In Vitro* at

- the Air-liquid Interface. *Part Fibre Toxicol*, 10:11.
<https://doi.org/10.1186/1743-8977-10-11>
68. Walter MN, Kohli N, Khan N, *et al.*, Human Mesenchymal Stem Cells Stimulate EaHy926 Endothelial Cell Migration: Combined Proteomic and *In Vitro* Analysis of the Influence of Donor-donor Variability. *J Stem Cells Regen Med*, 11:18.
<https://doi.org/10.46582/jsrm.1101004>
69. Yang Z, Yang X, Xu S, *et al.*, 2017, Reprogramming of Stromal Fibroblasts by SNAI2 Contributes to Tumor Desmoplasia and Ovarian Cancer Progression. *Mol Cancer*, 16:1–15.
<https://doi.org/10.1186/s12943-017-0732-6>
70. Ng WL, Yeong WY, Naing MW, 2017, Polyvinylpyrrolidone-Based Bio-Ink Improves Cell Viability and Homogeneity during Drop-On-Demand Printing. *Materials*, 10:190.
<https://doi.org/10.3390/ma10020190>
71. Ng WL, Goh MH, Yeong WY, *et al.*, Applying Macromolecular Crowding to 3D Bioprinting: Fabrication of 3D Hierarchical Porous Collagen-based Hydrogel Constructs. *Biomater Sci*, 6:562–74.
<https://doi.org/10.1039/c7bm01015j>
72. Wu J, Wang Y, Liu G, *et al.*, 2018, Characterization of Air-liquid Interface Culture of A549 Alveolar Epithelial Cells. *Braz J Med Biol Res*, 51:e6950.
73. Meenach SA, Tsoras AN, McGarry RC, *et al.*, 2016, Development of Three-dimensional Lung Multicellular Spheroids in Air-and Liquid-interface Culture for the Evaluation of Anticancer Therapeutics. *Int J Oncol*, 48:1701–9.
<https://doi.org/10.3892/ijo.2016.3376>
74. Abdelwahab EM, *et al.*, 2019, Wnt Signaling Regulates Trans-differentiation of Stem Cell Like Type 2 Alveolar Epithelial Cells to Type 1 Epithelial Cells. *Respir Res*, 20:1–9.
<https://doi.org/10.1186/s12931-019-1176-x>